

RESEARCH ARTICLE

10.1002/2017JC013011

Variability of the subtropical mode water in the Southwest Pacific

Denise Fernandez¹ , Philip Sutton¹, and Melissa Bowen² ¹National Institute of Water and Atmospheric Research, Wellington, New Zealand, ²School of Environment, University of Auckland, Auckland, New Zealand

Key Points:

- The variability of Subtropical Mode Water north of New Zealand was investigated from temperature observations
- The water mass has a short lifespan with little persistence from 1 year to the next one
- Deeper mixed layers and a deepening thermocline lead to increased mode water inventories

Correspondence to:

D. Fernandez,
Denise.Fernandez@niwa.co.nz

Citation:

Fernandez, D., P. Sutton, and M. Bowen (2017), Variability of the subtropical mode water in the Southwest Pacific, *J. Geophys. Res. Oceans*, 122, 7163–7180, doi:10.1002/2017JC013011.

Received 20 APR 2017

Accepted 17 AUG 2017

Accepted article online 25 AUG 2017

Published online 7 SEP 2017

Abstract The variability of Subtropical Mode Water (STMW) in the Southwest Pacific is investigated using a 28 year-long time series (1986–2014) of high-resolution expendable bathythermograph data north of New Zealand (PX06) and a shorter time series, the Roemmich-Gilson monthly Argo optimal interpolation for the 2004–2014 period. The variability in STMW inventories is compared to the variability in air-sea heat fluxes, mixed layer depths and transport of the East Auckland Current (EAUC) to assess both the atmospheric and oceanic roles influencing the formation and decay of STMW. The STMW north of New Zealand has a short lifespan with little persistence of the water mass from 1 year to the next one. Deeper mixed layers and negative anomalies in surface heat fluxes are correlated with increased formation of STMW. The heat content of the STMW layer is anticorrelated with inventories, particularly during the El Niño years. This suggests that large volumes of STMW are coincident with cooler conditions in the prior winter and less oceanic heat storage. There is significant seasonal and interannual variability in STMW inventories, however there are no trends in STMW properties, including its core layer temperature over the last decade. The variability of the winter EAUC transport is highly correlated with the STMW inventories and thermocline depth in the following spring, suggesting ocean dynamics deepen the thermocline and precondition for deeper mixed layers.

1. Introduction

Subtropical Mode Water (STMW) is a water mass typically found in each subtropical gyre, formed on the warm side of a western boundary current (WBC). The intense modification of water temperatures in western boundary regions leads to the formation of a lens of homogeneous water that moves away from contact with the atmosphere to a depth between the seasonal and permanent thermocline. Thus, STMW contains a history of ocean-atmosphere interactions and processes influencing the variability of the upper ocean circulation. STMW is characterized by low potential vorticity and minima in the vertical gradients of temperature and density [McCartney, 1982] resulting from weak stratification of the upper layers of the ocean [Hanawa and Talley, 2001]. Hence, the term “mode” implies that the water mass is relatively thick [Talley, 2011]. As with other water masses, the core of STMW forms at the surface [Iselin, 1939] before subducting along isopycnals ventilating the ocean interior where it slowly erodes as it is advected away from its formation region [Hanawa and Talley, 2001; Roemmich et al., 2005; Qiu et al., 2006]. All subducted water masses have important global climate implications, because the associated heat and dissolved CO₂ are effectively sequestered for the life of the water mass. Because volumes of STMW are indicators of heat storage and surface temperatures [Dong et al., 2007; Kelly et al., 2010; Rainville et al., 2014] STMW not only plays an important role as a heat reservoir [Hanawa and Talley, 2001] but also preserves a memory of surface conditions at the time the mode water was formed.

Previous studies have shown that fluctuations in STMW volume are correlated with variability in oceanic heat advection and air-sea heat fluxes [Sprintall et al., 1995; Roemmich et al., 2005; Dong et al., 2007] and with changes in stratification inherent to the state of WBCs [Qiu and Chen, 2006]. However, mesoscale activity can also influence volumes and longevity of STMW [Qiu et al., 2006; Kouketsu et al., 2012]. Moreover, variation in formation rates of STMW at interannual timescales has been linked to the El Niño/Southern Oscillation (ENSO) [Holbrook and Maharaj, 2008; Li, 2012] because of the relationship between ENSO and sea surface temperatures (SST). Recent interest in STMW variability has been linked to a more dynamic role, for example, in sustaining subsurface frontogenesis [Kobashi et al., 2006] and in modulating current

variability [Kobashi and Xie, 2013; Sasaki et al., 2012; Yu et al., 2015]. However, most of these recent studies focus on mode waters of the Northern Hemisphere where the WBCs are more energetic than their Southern Hemisphere counterparts.

Water with relatively low stratification and weak vertical temperature gradients has been detected in the Southwest Pacific, particularly in the Tasman Sea and the East Auckland Current (EAUC) region north of New Zealand [Roemmich and Cornuelle, 1992; Sprintall et al., 1995; Roemmich et al., 2005; Tsubouchi et al., 2007; Holbrook and Maharaj, 2008]. The STMW in the Tasman Sea has been linked to the presence of eddies depressing the thermocline which preconditions for the development of deeper mixed layers [Hu et al., 2007]. However, deeper mixed layers and larger volumes of STMW have also been linked to changes in the heat advected by the adjacent East Australian Current (EAC) [Wang et al., 2015]. Tsubouchi et al. [2007] show that long-term variations of STMW in the Tasman Sea are linked to the variability of the EAC. However, the STMW north of New Zealand has shown temporal variability distinct to that observed near the EAC [Tsubouchi et al., 2007] for reasons that are not clear and need further investigation. Therefore, the Southwest Pacific is a target region to study whether WBC variability has an impact on the formation and lifespan of STMW at seasonal, interannual and decadal time scales.

Here, we analyze upper-ocean temperature measurements over the last three decades to identify the variability of STMW north of the EAUC and investigate whether the causes of this variability are associated with the current. We also correlate fluctuations in regional air-sea heat fluxes with those observed in the mixed layer depth. High resolution expendable bathythermograph data (HRX) provide a record that is long enough (1986–2014) to study interannual and decadal changes in STMW inventories. Results over this region are compared with results from the shorter time series (2004–2014) of the Roemmich-Gilson monthly Argo optimal interpolation [Roemmich and Gilson, 2009].

This paper is organized as follows. In section 2, the various data and products are described and the methods for the calculation of STMW inventories are explained. In section 3, the mean distribution of the STMW and the variability at seasonal, interannual and decadal time-scales are described. Potential mechanisms explaining the observed fluctuations in STMW inventories are discussed in section 4. Finally, a summary of the main findings of this study are presented in section 5.

2. Data and Methods

2.1. Mixed Layer Depth

The upper ocean conditions that favour the formation of STMW are linked to the depth and extent of the wintertime mixed layer, typically quantified as mixed layer depth (MLD). The temperature and salinity homogenize in the mixed layer due to mixing processes such as wind-stirring and air-sea heat fluxes driving convection. A mixed layer is a uniform density layer characterized by low potential vorticity, in other words, weak stratification [Hanawa and Talley, 2001]. During winter, surface cooling followed by vertical mixing of the upper ocean leads to deeper mixed layers forming a water mass with weak temperature and salinity gradients: the STMW. In late spring and early summer, re-stratification of the water column isolates the STMW from the surface, and therefore from the atmosphere, and the mode water subducts into the permanent pycnocline.

Empirical methods to calculate MLD are based on temperature [Qiu and Chen, 2006; Tsubouchi et al., 2007] or density criteria [Huang and Qiu, 1994; Suga et al., 2004], or a combination of both using hybrid methods [de Boyer Montégut et al., 2004; Holte and Talley, 2009] depending on the patterns of stratification of the region of study. Here, the MLD is calculated as the depth at which the temperature changes by 0.5°C from that at the surface, similarly to previous MLD studies in the region [e.g., Holbrook and Maharaj, 2008]. No significant differences are found when the calculated MLD is compared with the MLD product from IFREMER/LOS Mixed Layer Depth Climatology downloaded from <http://www.ifremer.fr/cerweb/deboyer/mld>, despite the Ifremer-derived MLD climatology being based on a density threshold criterion, that is, when the density changes by 0.03 kg m^{-3} from the density measured at 10 m from the surface.

The annual climatology of the MLD in the South West Pacific region calculated from the Roemmich-Gilson Argo optimal interpolation is shown in Figure 1. Gradual deepening of the MLD starts in May with deeper mixed layers observed south of New Zealand. In July and August, mixed layers deeper than 100 m are

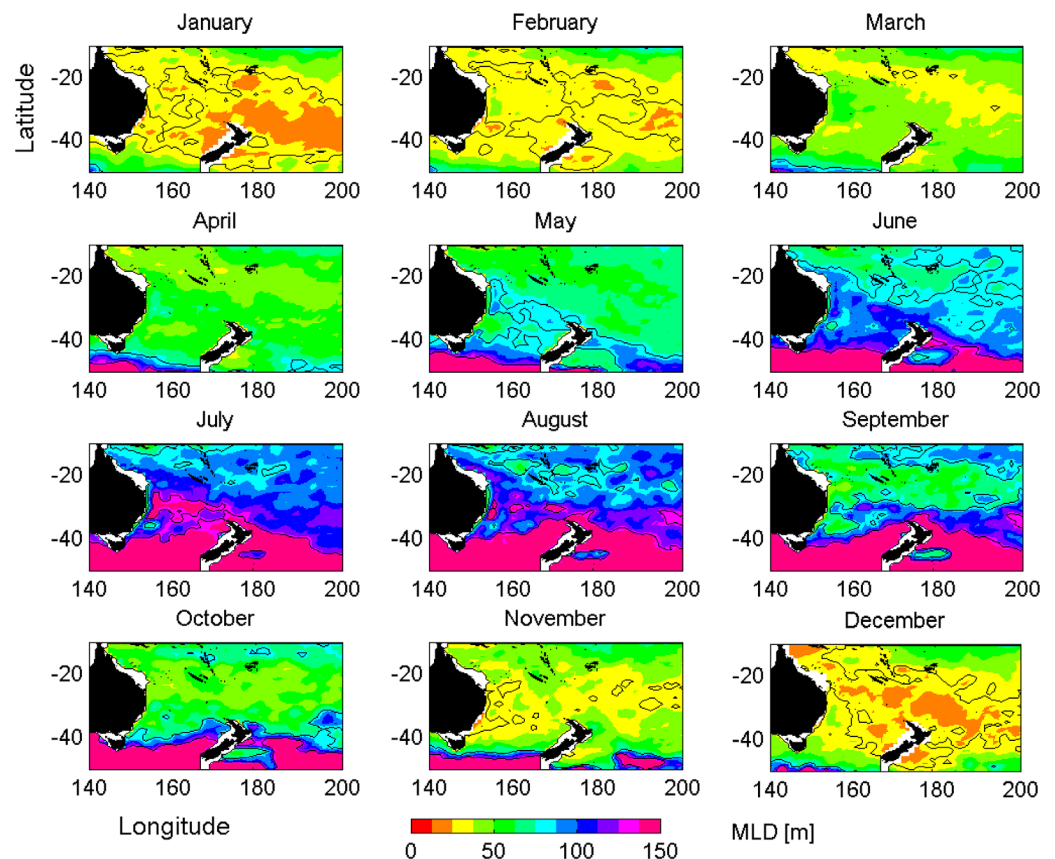


Figure 1. Mixed layer depths derived using the Roemmich-Gilson Argo optimal interpolation as the climatological monthly mean. The black lines are the 30, 80 and 130 m contour depth intervals.

observed east and north of New Zealand near 30°S. During the austral spring months of September and October the shoaling mixed layers have characteristic thickness of less than 40 m north of New Zealand [Sutton and Roemmich, 2001].

2.2. Identification of STMW and Inventories From Observations

Previous studies identified South Pacific STMW (SPSTMW) north of New Zealand and in the Tasman Sea region using a thermostad criterion, that is, using a critical value in the minimum of the temperature gradient [Roemmich and Cornuelle, 1992; Tsubouchi et al., 2007; Holbrook and Maharaj, 2008; Wang et al., 2015]. Here, the inventory of STMW is calculated using measurements of the upper ocean from two independent sets of observations.

The primary data used to identify STMW are from the 28 year long time series (1986–2014) of a repeat high resolution expendable bathythermograph section (hereafter HRX). Data along the PX06 line, connecting northern New Zealand and Fiji, consist of temperature measurements of the 0–800 m ocean recorded about four times a year from probes dropped from container ships. The data are bin-averaged into 10 m bins in the vertical with the maximum depth being approximately 800 m. The spatial resolution along the PX06 line is a profile every 10 kilometers in the boundary region and near the coast of Fiji, offshore of the 200 m isobath near the coast, and one profile every 30–40 kilometres in the open ocean. To reduce noise and to make these data comparable with other, lower resolution products, the HRX profiles were linearly interpolated into a 0.25° latitude grid along the PX06 line, and then smoothed spatially with a 3-point cosine filter. Differences in STMW inventories between the raw and filtered time series are statistically insignificant.

Following Roemmich and Cornuelle [1992], a vertical gradient in temperature was computed over 40 m intervals, and only those gradients with values less than 2°C/100 m, enclosed between the isotherms of 14° and

20°C and below the mixed layer, were selected to identify the location of the STMW. The inventory of STMW is defined as the total cross-sectional area (in km²) along the PX06 line.

In order to address potential biases due to irregular sampling of the seasonal cycle, the STMW inventories from the HRX data are compared with the Least-Square Harmonic Analysis (LSHA) of the same HRX temperature time series calculated by *Sutton and Roemmich* [2001] and updated for the period 1986–2015. The LSHA is a fit of basis functions (sines and cosines) that reconstruct the temperature signal at regular time and space intervals. The secondary product is the Roemmich-Gilson monthly Argo optimal interpolation [Roemmich and Gilson, 2009], which is used to identify STMW as an independent comparison with the HRX estimates. The Roemmich-Gilson product consists of optimally-interpolated Argo profiles on a 1° × 1° longitude and latitude grid (hereinafter RG OI). These are monthly anomalies of Argo-derived temperature and salinity fields over 58 pressure levels from the surface to 2000 m depth. The anomalies are referenced to a spatial mean of the fields over the period 2004–2014. Here, the absolute temperature and salinity values for the upper 2000 m were computed by adding the mean of the 2004–2014 period to the anomalies. While the RG OI has lower spatial resolution and spans only 10 years in comparison to the 28 years of HRX data, it is based on highly accurate measurements of temperature and salinity analyzed onto a regular temporal grid and has the advantage of geographic coverage over the entire Southwest Pacific ocean.

The vertical temperature gradient was calculated using centred finite differences along 176.5°E, which is the meridian closest in location to the PX06 line. The same threshold values in temperature and dT/dz as used in the HRX data set were applied to the RG OI. Inventories of STMW derived from the RG OI are below the MLD (the depth at which the sea surface temperature changes by 0.5°C).

2.3. Net Heat Flux and Ocean Heat Content in the STMW

Changes in the MLD and STMW inventories were correlated with ocean heat loss and gain because of the impact of heat flux on SSTs, which in turn play an important role in the development of the mixed layer. Here, the net heat flux data are provided by the Japanese 55 year Reanalysis (JRA-55; [Kobayashi et al., 2015]), made freely available from the Japanese Meteorological Agency (JMA) at <http://jra.kishou.go.jp/JRA-55/>. The monthly means of the short-wave radiation (q_s), long-wave radiation (q_l), latent heat (L) and sensible heat (S) were summed (equation (1)) to compute the net surface heat flux (Q_n). Then, a time series of Q_n was created by calculating an average along the 176.25°E meridian (nearest to 176.5°E), between 30°S and 33.75°S, where the STMW is found.

$$Q_n = q_s + q_l + L + S \tag{1}$$

In order to investigate how changes in the heat content of the upper ocean influence the STMW, the ocean heat content along the section (measured in J m⁻²) is calculated from both the HRX data and the RG OI by vertically integrating the temperature between the mean depths of the 14°C and 20°C isotherms using equation (2):

$$OHC = \int_{\bar{z}_{14}}^{\bar{z}_{20}} \rho c_p T dz \tag{2}$$

where \bar{z}_{14} and \bar{z}_{20} are the mean depths of the 14°C and 20°C isotherms, ρ and c_p are the potential density and specific heat of seawater respectively and T is the temperature. Density is a function of T , S and pressure while c_p is a function of T and S . For the RG OI, the OHC was calculated similarly along the 176.5°E meridian. In the case of the HRX data, ρ and c_p are taken as mean reference values (1024 kg m⁻³ and 4000 J kg⁻¹ °C⁻¹ respectively) because of the lack of salinity measurements in the HRX data set. Mean values of ρ and c_p from the RG OI are similar to these reference values. While \bar{z}_{14} and \bar{z}_{20} vary with location there is no significant change in the results when the integration is calculated between the average depths of 40 m for \bar{z}_{20} and 290 m for \bar{z}_{14} , hence the OHC represents changes in heat content over a fixed area. A time series of OHC is obtained by averaging the OHC values over the 28.5°–34.5°S latitude range, which covers the STMW region well. The temporal mean was removed from the OHC values because only the changes in OHC are of interest here. Hereafter, the time series of OHC represents the OHC anomalies.

2.4. Sea Surface Temperature and Core Layer Temperature of the STMW

Here the NOAA Optimum Interpolation (OI) Sea Surface Temperature (SST) V2 product was used to find the location of the 14°–20°C isotherm range at the ocean surface for comparison with the surface heat fluxes over the same region. The SST, provided by the NOAA/OAR/ESRL PSD, Boulder, Colorado, USA, from their website at <http://www.esrl.noaa.gov/psd/>, are the monthly means between January 1982 and December 2014 and have a spatial resolution of one degree in latitude and longitude [Reynolds *et al.*, 2007].

To describe the fluctuations of the characteristic temperature of the STMW, the core layer temperature (CLT) is calculated from the RG OI. The CLT is defined as the temperature at the location of the thermostad, that is, the minimum dT/dz . The CLT has been calculated along the 176.5°E meridian and spatially averaged between 28.5°S and 34.5°S to make it coincide with the location of STMW inventories along the PX06 line. The CLT is a useful property of the STMW because the temperature is set when the STMW forms [Taneda *et al.*, 2000]. The year-to-year variability of the STMW CLT is examined and then compared to the time series of the MLD and STMW inventories. The comparison shows simultaneous fluctuations in the inventories and properties of the STMW and the variability of the MLD. In addition to the CLT, the mean temperature of the STMW, i.e., the average temperature of the layer that defines the STMW, is calculated and compared to the CLT and MLD time series. The mean temperature of the STMW offers the advantage that temperature is not tied to an absolute minimum value (the thermostad), making the comparison useful to investigate consistency between the two methods.

2.5. Transport of the East Auckland Current

The transport of the EAUC was derived from along-track absolute dynamic topography (ADT) from Archiving, Validation, and Interpretation of Satellite Oceanographic data (AVISO). The ADT are measurements from Topex/Poseidon, Jason-1 and Jason-2 missions, at 10-day intervals for the period January 1993 to December 2013. First, surface geostrophic velocities were calculated as $u_s = -\frac{g}{f} \frac{\partial h}{\partial l}$, where $\frac{\partial h}{\partial l}$ is the ratio between changes in sea surface height h and along-track distance l (approximately 31 km), g is the gravity force and f is the local Coriolis parameter. Second, to calculate the absolute transports, information of the subsurface velocity field is needed. This consisted of *in situ* Conductivity, Temperature and Depth (CTD) profiles giving a measurement of the current shear through the water column. Finally, absolute transports, measured in Sverdrups ($1\text{ Sv} = 10^6\text{ m}^3\text{ s}^{-1}$) and based on the altimetry and information of velocity changes with depth, are derived from the surface geostrophic velocities and the shear over the width of the EAUC. For details in the calculations see Fernandez [2017].

2.6. Statistical Significance of the Correlations

The correlation coefficients (r) are reported either with their corresponding level of significance p (p -value) or confidence level. The p -value gives the probability that r is obtained by random chance. In order to calculate a p -value the number of degrees of freedom (DOF) in the time series needs to be established. To find the DOF, the autocorrelation function of each time series is calculated as a function of time-lags. Then, the decorrelation time D is the first-zero crossing indicating that the variable is no longer autocorrelated [Emery and Thomson, 2001]. The effective number of DOF, i.e., the number of independent realizations, can then be calculated by dividing the length of the time series ($N\Delta t$) by the decorrelation time (D) as $DOF = \frac{N\Delta t}{D}$ [Von Storch and Zwiers, 2001]. A two-tailed t -test is used to determine the p -value. The two-tailed test is a more conservative approach than the one-tailed test and is preferred as there is no a priori direction of a specific effect.

3. Results

3.1. Mean Distribution of STMW

The mean STMW thickness over the 2004–2014 period from the RG OI is shown in Figure 2. STMW inventories thicker than 100 m are distributed zonally from 150°E to 180° across the Tasman Sea and to the east of New Zealand, and meridionally from 25°S to just over 35°S. Thickness decreases abruptly east of the Kermadec Ridge near 180°. Superimposed on the mean thickness map are the mean steric height contours (calculated from the RG OI) for the 180 m level referenced to a pressure level of 2000 m ($h_{180/2000}$), to give an indication of the mean flow at 180 m. In the Tasman Sea, STMW thickness generally follows steric height contours. The abrupt change in thickness east of Kermadec Ridge also coincides with steric height contours

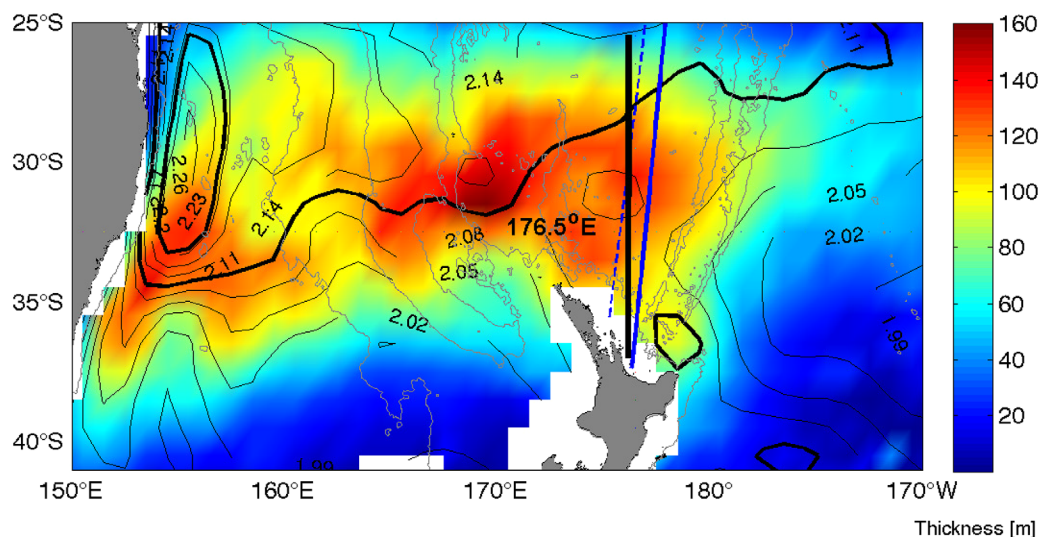


Figure 2. Mean STMW thickness calculated over the period 2004–2014 using the RG OI. The PX06 line prior to 1999 (dashed blue) is the Auckland-Suva transect, more recent sections are between Tauranga-Suva (solid blue). The black line at 176.5°E corresponds to the closest meridian to the PX06 line. The black contours are steric height at 180 m referenced to 2000 m and the contour interval is 0.03 m. The 2.11 m steric height contour separates two maxima in STMW thickness. The grey thin contour represents the 2000 m isobath.

warping to follow the ridge orientation in the 30°–35°S latitude range. Between 167°E and 180° two maxima in thickness are located east and west of the 2.11 m steric height contour (thick black line) in a double core structure (also observed by *Tsubouchi et al.* [2007]). Here, the focus is on the STMW core southeast of the 2.11 m steric height contour, not only because it is immediately adjacent to the western boundary region off New Zealand but also because it is transected by the PX06 line.

3.2. The Seasonal Cycle of STMW

A seasonal climatology of STMW from the 2004–2014 RG OI is shown in Figure 3. STMW thickness gradually decreases from January to June and increases from July to October primarily around 30°S and west of 180°, reaching a maximum of about 180–200 m in October. From November on, thickness contracts again to reach the austral summer conditions observed in January.

The seasonality of STMW inventories from the HRX and the RG OI are shown in Figure 4a. The shaded areas are the standard errors $ste = \frac{\sigma}{\sqrt{N}}$, where σ is the standard deviation of the time series for each month and N is the number of HRX transects available in each month. All the HRX measurements are displayed to show the spread from the mean value. Similarly, the individual monthly values are shown for the RG OI.

From the HRX data, STMW inventories along the PX06 line decay from December to May, and increase from July to November. The seasonal cycle calculated with the LSHA updated from *Sutton and Roemmich* [2001] has a smoother decay in the summer-autumn seasons than the HRX data set, but a similar pattern overall. The annual variability is also captured by the RG OI. During the formation period, from August to October, both estimates are statistically similar, despite the fact that the averages are calculated over time series with different lengths. From both HRX and RG OI it is estimated that STMW inventories decrease between 50% and 75% respectively from spring to the following winter (between October and August).

The vertical structure of the STMW seasonal cycle is shown in Figure 4b. The dT/dz is calculated along the meridian 176.5°E and averaged for the latitude range 28.5°–34.5°S. The smallest gradients, bounded by the 14°–20°C isotherms (bold black lines), are found between 170 m and 250 m. In the climatological average, the MLD (thick red line) is deeper in July reaching approximately 100 m.

3.3. Interannual Variability of STMW Properties and Inventories

In this section, fluctuations in potential temperature (θ) and salinity (S) of the STMW from the RG OI are investigated in order to observe whether changes in the properties of the water mass have occurred or there are significant trends. We have used θ instead of the measured temperature (T) to be consistent with previous analyses of θ - S relationship in the Southwest Pacific [e.g., *Tsubouchi et al.*, 2007].

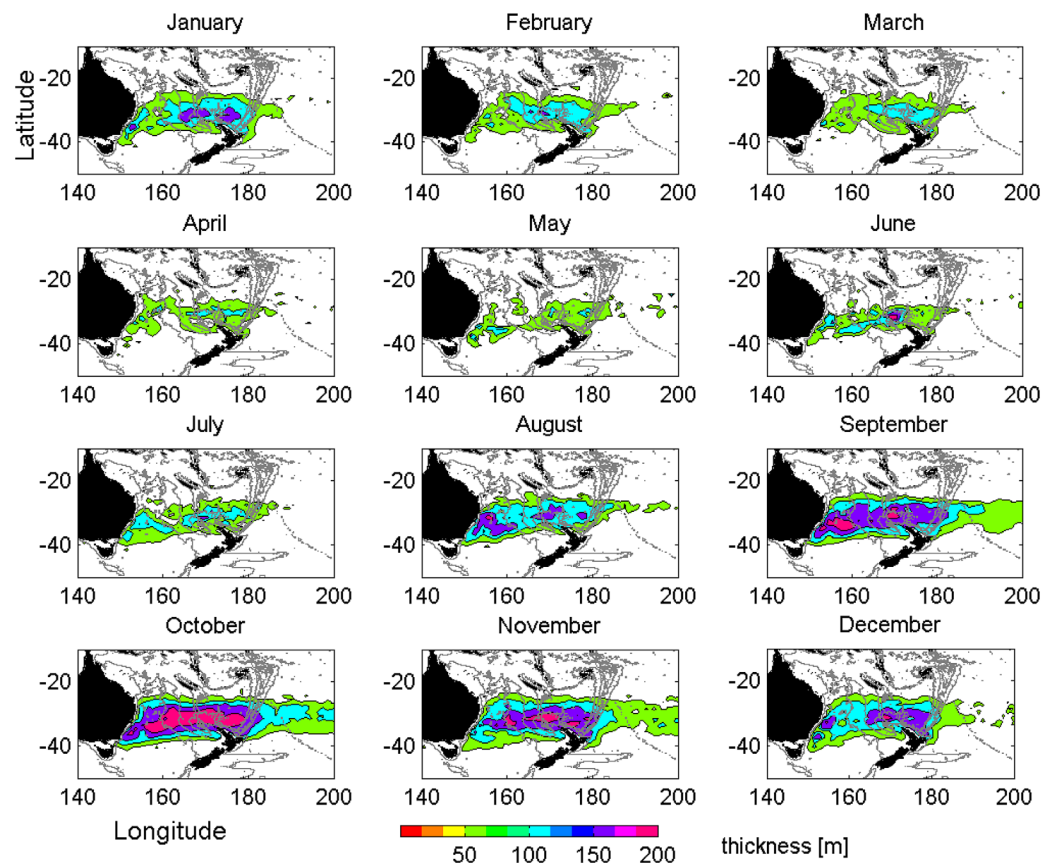


Figure 3. Climatology for thickness of STMW as defined by the thermostat method applied to the RG OI. The gray line indicates the 2000 m isobath.

Figure 5a shows a θ - S diagram using the RG OI identifying STMW in the region delimited by 28.5° - 34.5° S, 173° E- 180° . The region is chosen based on the mean distribution of STMW (Figure 2) and on the wintertime SST when surface isotherms for the 14° - 20° C range are located within the 28.5° - 34.5° S latitude band (see inset Figure 5a).

Temporal changes in the properties of STMW are analyzed by calculating annual averages for the period 2004–2014. The STMW lies in the potential density range $\sigma_{\theta} = 25.25$ – 26.5 kg m^{-3} range with a core density of $\sigma_{\theta} = 26 \text{ kg m}^{-3}$. Figure 5b shows temperatures and salinities bin-averaged over 0.5° C intervals and then annually averaged. The STMW exhibits substantial interannual variability at all depths. It appears that changes in salinities are larger in the 17° - 20° C layer, ranging from 35.65 psu during 2005–2007 (saltier STMW) to 35.5 psu in 2008–2009 (fresher STMW). Thus, while there is significant variability, there is no simple trend in salinity through the sampling period.

The autocorrelation functions of the mean temperature and salinity of the STMW are shown in Figure 6. Both properties show a fast decay in the autocorrelation with an e-folding time of less than 1 year. A decorrelation time shorter than an annual cycle suggests that properties of the STMW are renewed each year.

Figure 7a shows time series of the MLD, the CLT and the mean temperature of the STMW. The MLD is deepest in July–August and shallowest in December–January. It is noted that the mean temperature of the STMW is highly correlated with the CLT ($r = 0.94$, $p < 0.001$). The interannual variability is difficult to analyze because the seasonality dominates the fluctuations of the MLD, with the seasonal cycle remaining almost constant throughout the 11 year period. This is not the case for the CLT variability, which shows amplitude changes throughout the 11 years. Removing the seasonal cycles exposes the much smaller interannual signal in CLT, mean temperature and MLD (Figure 7b). At interannual time scales, the CLT and the MLD are uncorrelated ($r = 0.05$). The correlation of CLT with STMW inventories at interannual time scales (not shown)

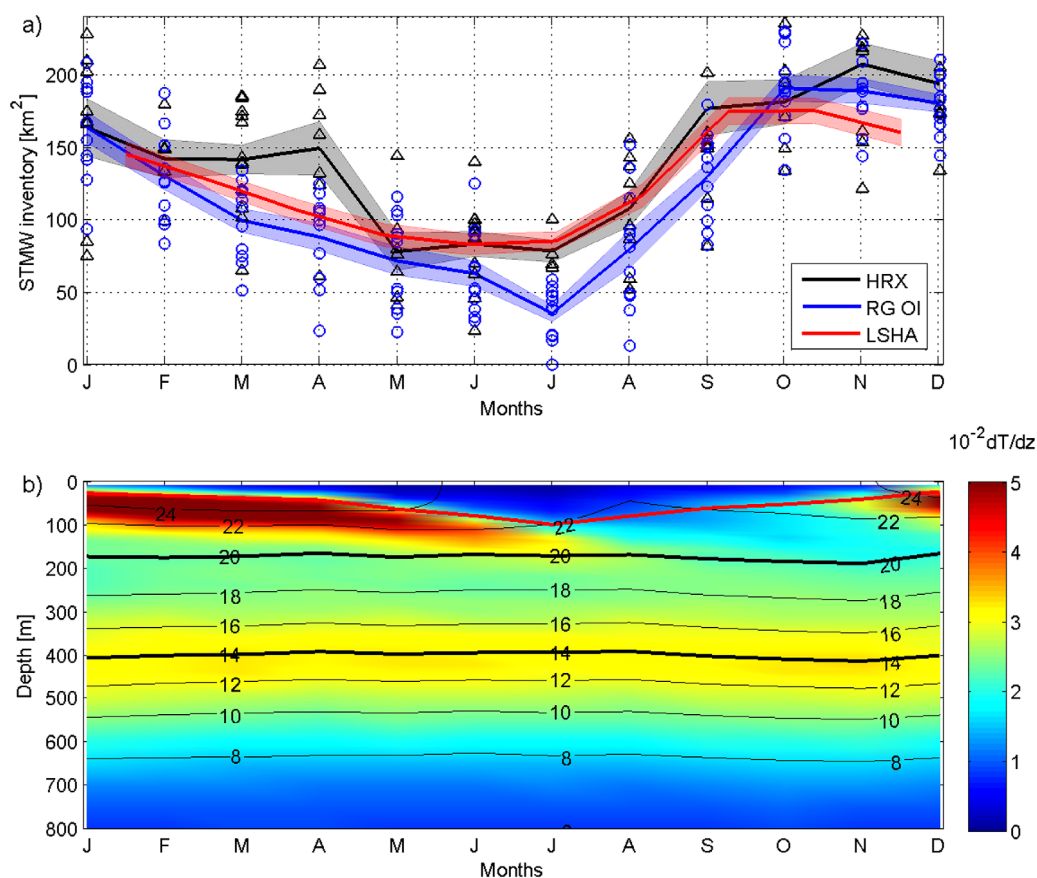


Figure 4. (a) Seasonal climatology for the inventories of STMW along the coordinates of the PX06 transects (HRX and LSHA) and along 176.5°E (RG OI). Shaded areas are the standard error for the means taking into account the number of transects for each individual month in the case of the HRX data and 10 years of data in the case of the RG OI. Individual measurements of the HRX (triangles) and RG OI (circles) are displayed to show the distribution of data. (b) The vertical structure of the STMW seasonal cycle shown as the thermocline (dT/dz), from the RG OI. The red line is the seasonal MLD and the black lines are the isotherms with the 14°C and 20°C highlighted.

is negative and weak ($r = -0.13$) suggesting once again that there is no clear correspondence between changes in STMW inventory and changes in its water mass properties.

3.4. Low-Frequency Variability of STMW Inventories

To focus on the low frequency variability, STMW anomalies are calculated by removing the corresponding seasonal cycles from both the HRX and the RG OI time series (Figure 8). While the RG OI is only 11 years long, making it quite short to study signals with periods longer than 5 years, the time series is still useful to include in the analysis as an independent comparison with the HRX in the overlapping period. Each time series was low-pass filtered to further remove fluctuations with periods less than a year (the HRX with a 5-point window assuming 4 transects a year and the RG OI with a 15 month cosine filter). The greatest variation in STMW inventories occurred between the 1990s and 2000s, with the minimum in 1990 and maxima in 1996 and 1998. During the RG OI era (2004–2014) the frequency in the variability increases, with inventories peaking around every 5 years and a similar pattern of variability being observed in both products for the period 2004–2012.

While the longer time series shows some signs of a decadal signal over the first two decades, it does not persist after 2000, when the variability in inventory becomes weak and higher in frequency.

3.5. Net Surface Heat Fluxes and Changes in the Mixed Layer

In order to understand whether the causes of changes in the MLD are potentially due to ocean-atmosphere interaction, the Q_n values in August (austral winter) are compared to the MLD when SSTs are, on average, the lowest. Figure 9 shows a near linear relationship between the winter MLD and Q_n . The negative slope of

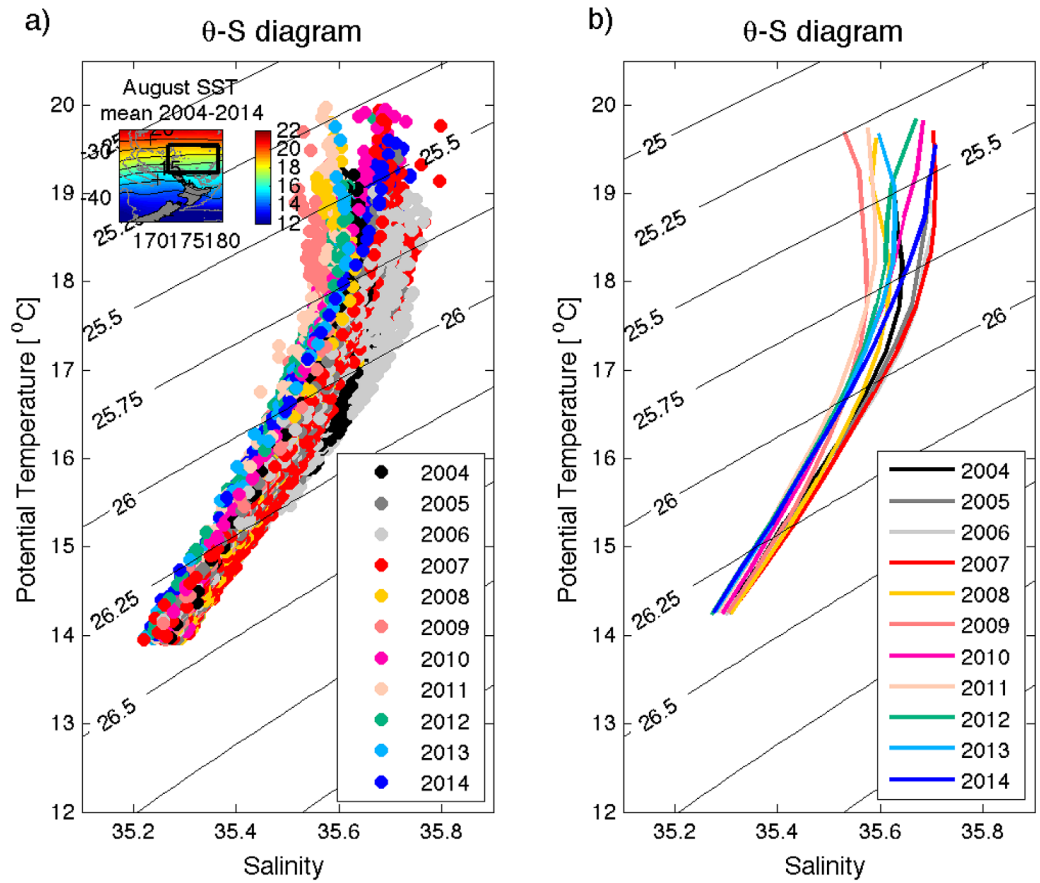


Figure 5. θ -S diagram of STMW in the box shown in the inset, from the RG OI (a) for the period 2004–2014 and (b) bin-averaged every 0.5°C temperature and then annually averaged.

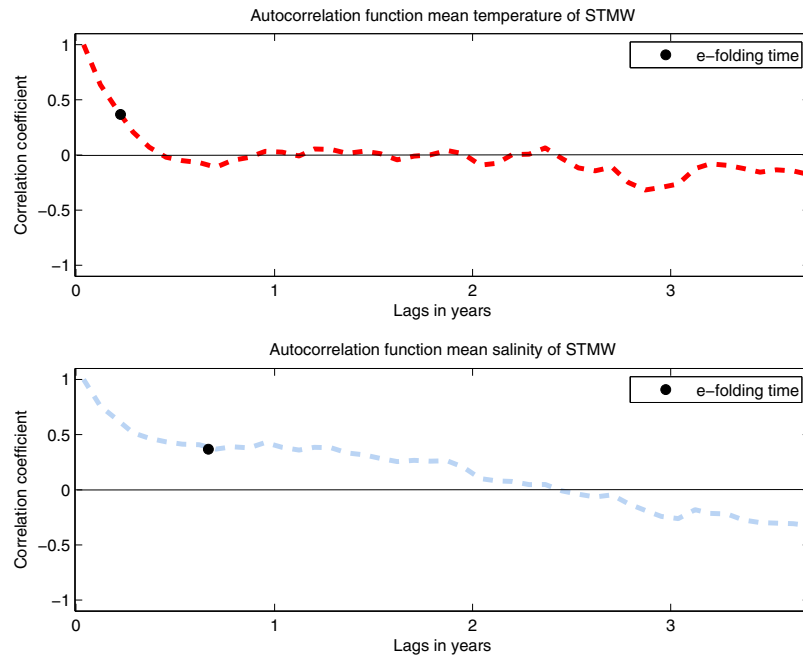


Figure 6. Autocorrelation function of (a) the mean temperature and (b) the mean salinity of the STMW from the RG OI, as a function of lags (in years).

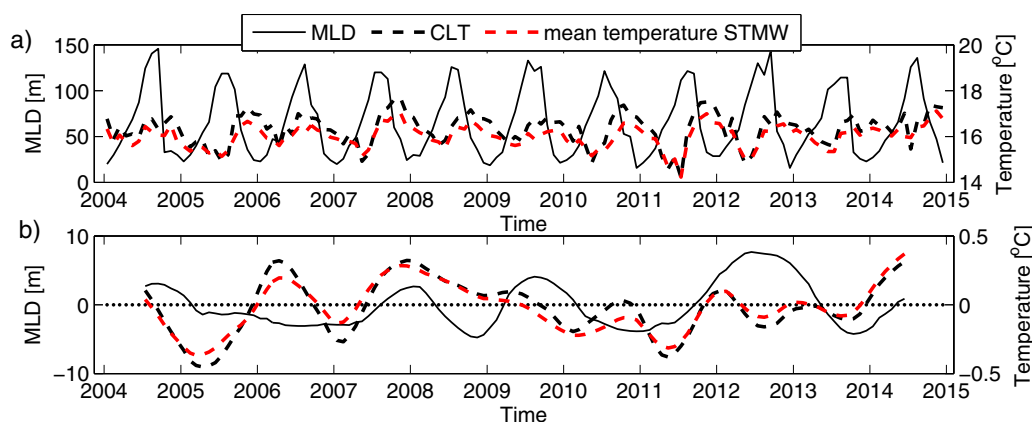


Figure 7. (a) Time series of MLD, CLT and mean temperature of STMW from the RG OI. (b) As for Figure 7a but deseasoned and smoothed with a 15 month cosine filter.

the line indicates that a greater ocean heat loss in the region is concurrent with deeper mixed layers during the coldest month of the year. To account for the variance in both the x and y variables, we use principal component analysis because it uses an orthogonal transformation where the slope of the line that fits the observations accounts for as much of the variability in all of the data as possible [Emery and Thomson, 2001].

3.6. Ocean Heat Content Anomalies and STMW Inventories

The annual cycle of OHC of the layer with mean 14°-20°C isotherm range ($\bar{Z}_{20}-\bar{Z}_{14}$) for the STMW region is shown in Figure 10a. For both the HRX and RG OI data sets, the OHC is higher in April, when approximately 50% of the STMW formed in the previous winter along the PX06 line and 176.5° meridian has vanished (see Figure 4). From August to October the heat deficit is maximum, coinciding with the period of STMW formation, which reaches a peak in October-November. The amplitude of the annual cycle appears to be larger in the HRX than in the RG OI, but the temporal pattern is similar: the OHC is maximum in autumn and minimum in late winter.

Using the shorter time series from the RG OI, the interannual variability of the OHC time series is compared to the STMW inventories in Figure 10b. Here, the annual cycle was removed from both time series and they were low-pass filtered to remove fluctuations shorter than 15 months. The signals are negatively correlated ($r = -0.48$, $p = 0.1$), indicating that STMW inventories are in general larger when there is less heat in the 14°-20°C layer. This anti-correlation suggests that increased inventory of STMW is a reservoir for water that is uniformly cooler.

3.7. Relationship Between MLD, SST, and STMW Inventory

Time series of MLD, SST and STMW inventory are compared to test the hypothesis that deeper winter mixed layers are a key factor in producing more STMW (Figure 11). Here, the HRX data and the SST reanalysis are

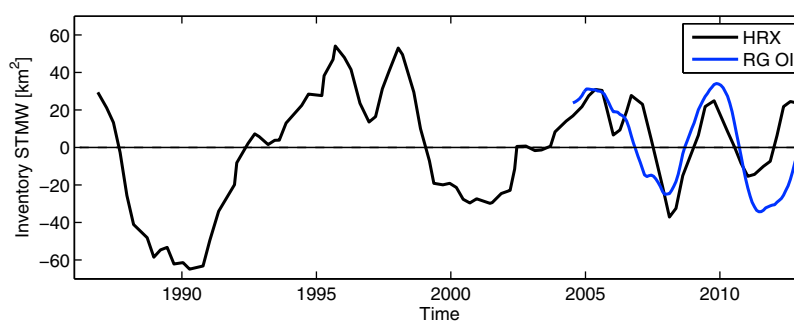


Figure 8. Time series of STMW inventories (km^2). Black curve correspond to the inventories derived from the HRX data, blue curve from the RG OI. To show the low-frequency signal, both time series were deseasoned and smoothed to remove signals with periods shorter than annual.

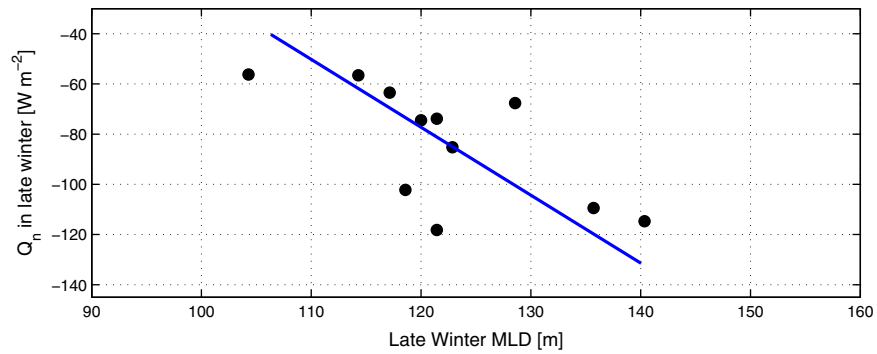


Figure 9. Scatter plot of Q_n and MLD in late winter. The blue line with a negative slope is the regression using principal component analysis and accounts for the variance in both the x and y variables.

used because of their long records (1986–2014). Note that to investigate the relationship between late winter mixed layer and STMW inventories in spring, only years with available HRX measurements in the corresponding seasons were included. There is a high correlation ($r = 0.78$, $p = 0.002$) between the late winter (August or September) MLD and STMW inventories in the following spring season (October or November). Conversely, SSTs are anti-correlated to both the STMW inventory ($r = -0.6$, $p = 0.04$) and the MLD ($r = -0.48$, $p = 0.1$) over the same period. These relationships support the hypothesis that larger STMW inventories are associated with preceding cooler SSTs and deeper mixed layers.

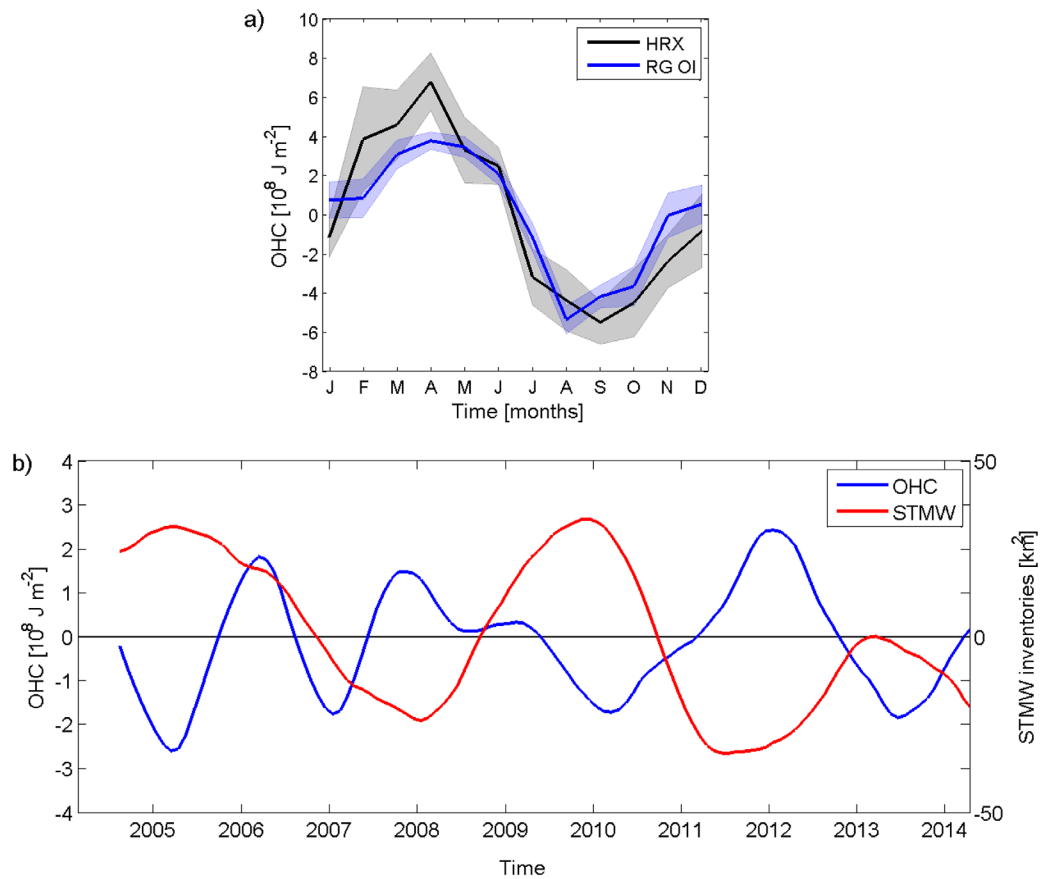


Figure 10. (a) Seasonal cycle of the OHC derived from the HRX data (black curve) and the RG OI (blue curve). Shaded area represents the standard error with N based on the number of transects for each month of the HRX data set and on 11 years of measurement for RG OI. (b) Time series of OHC and STMW inventories from RG OI over 176.5° meridian with the seasonal cycle removed and smoothed with a 15 month cosine window.

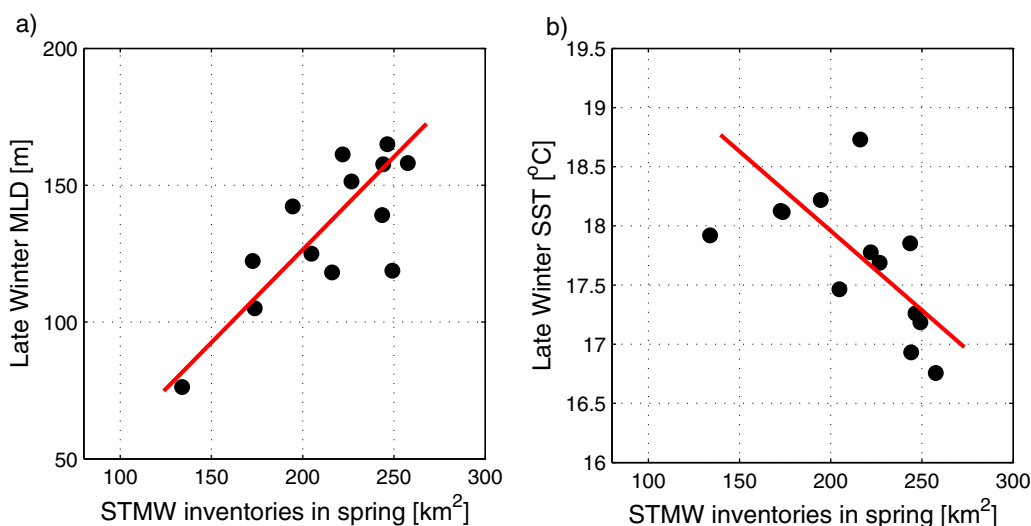


Figure 11. Scatter plot of the STMW inventories in spring and (a) the late winter MLD and (b) the late winter SST. The STMW and MLD are correlated with $r = 0.78$ based on $N = 13$ years depending on availability of data. The SST is anticorrelated with the STMW with $r = -0.6$.

The previous results indicate that the MLD has an influence on STMW production. On a short-time scale, variations in heat content of the upper ocean may be an important factor in determining mixed layer depths. Dynamics below the mixed layer affect the upper ocean stratification and will impact the mixed layer depth, for example high (low) stratification will lead to shallow (deeper) mixed layers.

3.8. ENSO Impact on STMW Inventories

The influence of ENSO events and fluctuations in STMW is analyzed by comparing the Southern Oscillation Index (SOI) time series with the annually-averaged and deseasoned time series of the STMW inventories.

Previous studies have shown that the SOI is significantly correlated with SSTs, with cooler SSTs around New Zealand during the El Niño [Greig et al., 1988; Mullan, 1998; Goring and Bell, 1999; Sutton and Roemmich, 2001] which would be expected to reflect the development of deeper mixed layers. Figure 12 shows the 28 year record of both the STMW inventories and the SOI, with the shorter RG OI record included for comparison. To make the correspondence between ENSO and STMW inventories more evident, the STMW axis is flipped to be positive downward and the inventory time series was interpolated to the same time grid as the SOI (monthly values). The correlation for annual averages of both the HRX

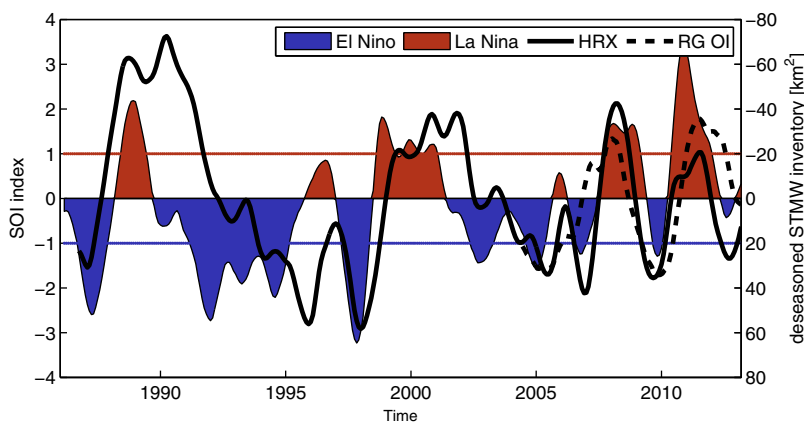


Figure 12. Comparison of monthly interpolated STMW inventories and the SOI. The HRX (solid black curve) and the RG OI (dashed black curve) time series have the annual cycles removed. All the time series were smoothed with a 15 month cosine window.

and SOI time series is negative ($r = -0.34$, $p = 0.08$) at zero-lag. There is a general tendency for greater inventories to occur in the El Niño years. Conversely, less than average inventories occur in warmer ocean conditions during La Niña. The largest changes in STMW inventories, which occurred during the late 1980s and late 1990s, coincide with La Niña in 1988/1989 and the strong El Niño in 1997/1998. Fluctuations in STMW inventories after the year 2000 are predominantly in phase with those of the SOI, however it seems there is no clear relationship between the magnitude of the ENSO events and the changes in inventories.

The correlation between SOI and OHC (not shown) is positive ($r = 0.40$, $p = 0.03$), which is consistent with previous results that during the El Niño years greater STMW inventories are in phase with cooler conditions and greater ocean heat loss.

3.9. Western Boundary Current Transport and STMW Inventories

A connection between the boundary currents and the STMW inventories is also investigated, since the variability of transports may change the water properties accumulating on the northern side of the currents [Hanawa, 1987]. This analysis focuses on the relationship between the STMW inventories, the transports along the northern boundary of New Zealand and the variability of the depth of the thermocline in the same region, defined as the depth of the 12°C isotherm (z_{12}). This threshold, which is below the mixed layer depth, is chosen as a descriptor of the large-scale surface circulation while being independent of the definition of the STMW (i.e., outside the 14°–20°C range).

Firstly, to evaluate a potential connection, the time series of the STMW inventories is compared with a time series of the volume transport associated with the EAUC (Figure 13). The unfiltered time series are shown as thin grey and red lines for the STMW inventories and transport respectively in Figure 13 while the thick black and red lines represent the annually smoothed time series. The correlation between the interannual variability in transports and STMW inventories is $r = 0.51$ ($p = 0.02$) at zero-lag, suggesting that increased STMW inventories occur with increased transport of the EAUC.

One possible mechanism linking changes in STMW inventories to the western boundary current transport may be deepening of the thermocline on the offshore side of the current creating favourable conditions for the development of deeper mixed layers.

Secondly, we compare the EAUC transport, the STMW inventories and z_{12} for the years when there are available data for winter and spring (of the same year). The largest correlation between z_{12} and the EAUC is obtained when transport leads z_{12} by one season as shown in Figure 14. The time series are positively correlated ($r = 0.9$, $p < 0.001$) suggesting that the thermocline variability in spring follows the changes in the boundary current in the winter, when the formation and maximum inventories of STMW occur. In addition, there is a strong correspondence between winter transport and spring STMW inventories ($r = 0.62$, $p = 0.03$) with the result shown in Figure 13 but indicating that the correspondence is stronger with one season lag.

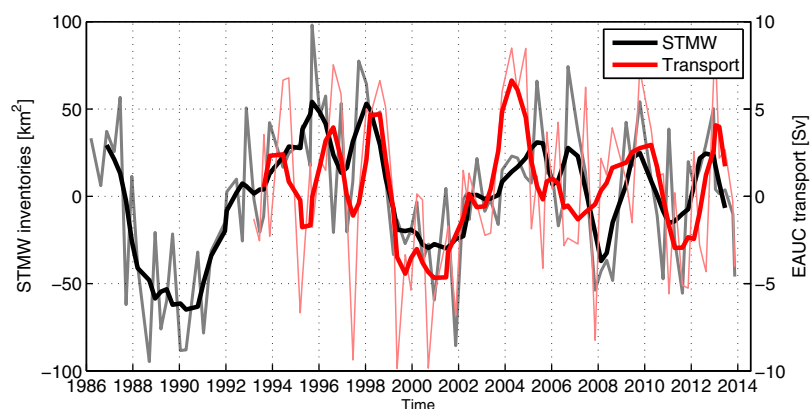


Figure 13. Time series showing the interannual variability in STMW inventories (anomalies in the thick black curve) and the western boundary current transport (anomalies in the thick red curve). Thin lines in matching colours are the unfiltered time series.

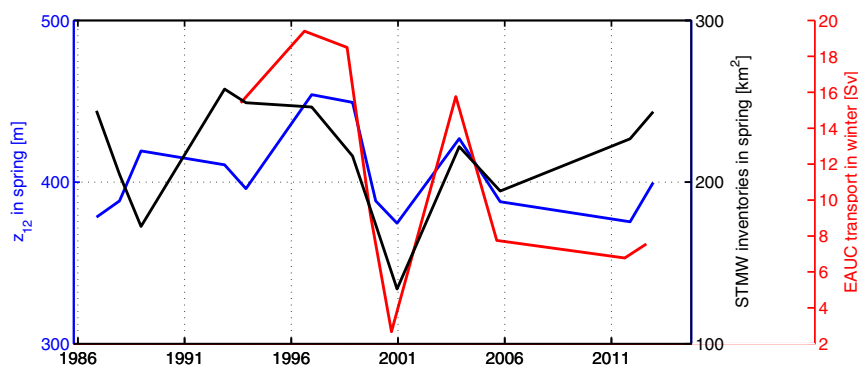


Figure 14. Comparison of z_{12} in spring, STMW inventories in spring and transport of the western boundary current in the prior winter. The EAUC transport has been lagged by one season with respect to the z_{12} and STMW inventories.

4. Discussion

STMW with mean thickness greater than 100 m is clearly observed across the Tasman Sea and north of New Zealand (Figure 2). The mean thickness distribution appears to be bounded by mean steric height contours, particularly in the Tasman Sea at 37°S and between 150°E – 180° . *Tsubouchi et al.* [2007] also compared the spatial distribution of STMW to the local circulation and find one maximum of STMW thickness at 175°E coincident with flows exiting to the central Pacific [*Tsubouchi et al.*, 2007]. However, our results showed that the distribution of STMW ends where steric height contours are nearly-meridional, consistent with early findings that STMW does not migrate further east than its formation region [*Roemmich and Cornuelle*, 1992].

On a seasonal time scale along the PX06 line, STMW inventories peak in October and November and are at a minimum from May through August with minimum values in June (LSHA), May and July (HRX) and July (RG OI) (Figure 4). These results are consistent with measurements of the seasonal cycle of STMW volumes over the whole Tasman Sea and the region north of New Zealand [*Holbrook and Maharaj*, 2008], suggesting that the seasonal cycle of STMW over the PX06 line is representative of the annual fluctuations over a broader region.

The STMW thickness reduces from a maximum in October–November to a minimum in June–July (Figure 3) indicating that persistence of STMW from previous years is limited. The short lifespan of South Pacific STMW is noted by *Roemmich and Cornuelle* [1992] who from a shorter HRX time series (1986–1991) estimated that STMW decreases by 50% between its maximum and minimum inventories in spring and autumn respectively. This estimate agrees with the decay in STMW inventories found here using the HRX data (the RG OI shows a larger decrease of 75%), with the difference that results here are estimated over a much longer period. A previous study found advection of STMW occurs in the recirculation region of the EAC [*Hu et al.*, 2007], however transport of STMW is limited to the north of the Tasman Front [*Zilberman et al.*, 2014]. Migration of STMW away from the EAUC to the east is implausible, as thickness decreases rapidly east of the Kermadec Ridge, as also shown by *Roemmich and Cornuelle* [1992]. Because the definition of STMW is not designed to follow water parcels, changes in the vertical temperature gradient can cause relatively large volumes of STMW to erode over a season.

Despite the strong seasonality observed in the STMW inventories, interannual variability is significant in both the properties and the amount of STMW formed each year. The STMW temperature and salinity relationship (θ - S), depicted in Figure 5b, indicates that interannual changes are more evident in the shallower part or top of the STMW corresponding to the 17° – 20°C temperature range, well above the interannual fluctuations in the CLT (ca. 15° – 17°C , Figure 7a). The mean value of the CLT is 16°C , which is also similar to the mean CLT of the South type of STMW from *Tsubouchi et al.* [2007], for the same region and from the HRX data set for the period 1986–2003. The lack of a simple pattern in the θ - S relationship and the absence of a trend in the time series of the CLT suggests that, while there is strong year-to-year variability, there are no significant trends in the properties of the STMW in the 2004–2014 period.

Interannual variability of the STMW inventories along the PX06 section and along 176.5°E is evident, particularly a decline in STMW inventories during the late 1980s. This decline was also observed by *Roemmich and*

Cornuelle [1992] and attributed to shallow winter MLDs caused by warmer conditions that led to stronger stratification and weak mixing. The recovery of inventories observed during the early 1990s is noted by Sprintall *et al.* [1995], particularly for the years 1992–1993 that were reported to be one of the coldest periods around New Zealand in nearly 50 years. The cooler atmospheric conditions were reflected also in colder oceanic subsurface temperatures that potentially contributed to enhanced wintertime mixing and hence deeper mixed layers [Sprintall *et al.*, 1995].

Larger inventories of STMW in the North Pacific have been found to be correlated with cooler CLT [Douglass *et al.*, 2013], while, conversely, there is no relationship between cooler STMW and increased inventories in the North Atlantic. Here in the Southwest Pacific, STMW inventories are poorly anticorrelated with CLT (not shown). Moreover, the lack of correlation between MLD and CLT (Figure 7b) suggests that while deeper mixed layers are a key factor for STMW formation, as shown in section 3.7, there is not necessarily an impact on the properties of the STMW.

To explore the causes of MLD changes, the STMW inventories are compared with the occurrence of ENSO events. Past ENSO events tend to impact air temperatures and SSTs around New Zealand [Mullan, 1998; Goring and Bell, 1999], and potentially MLD, SSTs and STMW inventories may be related to ENSO. Our results showed a negative correlation at zero lag ($r = -0.34$, $p = 0.08$) between the time series of SOI and STMW inventories, with some of the El Niño events in phase with increased STMW inventories. In particular, the El Niño phase of ENSO (negative SOI) is associated with cooler than normal SST, often attributed to increasing south-westerly winds [Gordon, 1986], although more recent work found a variety of potential mechanisms [Ciasto and England, 2011]. Anomalous cooling of the upper subsurface layers of the ocean (due to atmospheric, oceanic forcing or a combination of both) would lead to deeper mixed layers favouring the production of more STMW. Holbrook and Maharaj [2008] also found a correlation, i.e., $r = -0.3$ (95% significant), at 3 month lag between SOI and STMW volume, with STMW lagging the SOI. While remaining unconvinced about the robustness of the lag given the smoothing of the time series, they concluded that the El Niño phase of ENSO significantly contributes to thickening of the STMW volumes over the whole Tasman Sea region including north of New Zealand.

The upper-ocean heat content and heat flux were analyzed to investigate their influence on forming deeper mixed layers. Here, it is found that greater STMW inventories are directly related to deeper mixed layers at seasonal and interannual time scales. Deeper mixed layers are also correlated with greater net surface heat fluxes during winter (Figure 9). We have shown in Figure 10b that STMW inventories are anti-correlated with OHC, with less ocean heat content during periods of greater STMW inventories. This is consistent with the argument given by Kelly *et al.* [2010] describing mode waters as a “heat deficit reservoir,” with generally larger volumes of STMW occurring with cooler and less stratified upper-ocean conditions with less heat content. While we find STMW inventories in the Southwest Pacific are linked to negative heat content anomalies, weak relationships are found in other STMW regions, such as in the Kuroshio Current in the North Pacific, where there are no significant correlations between net surface heat fluxes, ocean heat content and STMW thickness [Rainville *et al.*, 2014]. Thus, it seems that the regional heat balance has some contribution on the STMW north of New Zealand in comparison to other ocean basins.

Low-frequency variability of STMW inventories corresponds with fluctuations observed in the transport of the EAUC, the subtropical western boundary current along northeastern New Zealand (Figure 13). The correspondence is greater when transports and inventories are compared with one season lag, that is, when transports in winter are correlated with STMW inventories in the following spring. The influence of a deeper thermocline will be at the end of winter when the transport of the EAUC coincide with deeper mixed layers, the STMW is forming and peak in the following spring, hence the one-season lag. To further explore the connection between transport of the EAUC and STMW inventories, the depth of the thermocline is compared to both the STMW and the transport (Figure 14). A deeper thermocline correlates well with a strong EAUC. This result suggests there might be a dynamic forcing preconditioning the formation of STMW in addition to the thermodynamic forcing from heat fluxes. A deeper thermocline has been proposed as the mechanism for the development of deeper mixed layers that favour the production of STMW in the Northwest Pacific [Sugimoto and Hanawa, 2010]. In the Kuroshio Current region, Qiu and Chen [2006] indicate that at interannual time scales, a dynamic forcing such as the state of a boundary current (where a stable/unstable state corresponds to low/high level of mesoscale variability), may be responsible for changes in STMW thickness. This relationship occurs because a stable current leads to a weakly stratified upper ocean,

hence, the development of deeper mixed layers that lead to increasing STMW inventories and vice-versa. However, a recent study in the western South Pacific by Wang *et al.* [2015] finds that the interannual variability of STMW is linked to the flow of the EAC via horizontal heat advection, with low heat transport leading to more production of STMW, particularly during the positive phase of SOI (La Niña). Here, we find that when the flows of the EAUC are stronger, the STMW inventories increase. This difference could be related to the fact that the STMW from Wang *et al.* [2015] is the “West-type” [Tsubouchi *et al.*, 2007], located near the EAC. The EAC is a larger boundary current than the EAUC, and it is possible that greater advection of heat in the EAC has a larger role in increasing stratification of the upper ocean and causing less favourable conditions for STMW formation.

The lagged correlation between winter transports and thermocline depths in spring may only explain the dynamic influence of the current on STMW inventories over shorter time scales. Enhanced STMW production would also be expected when both deeper mixed layers and increased transports of the EAUC combine.

Several further questions arise from the analysis of the formation and variability of STMW inventories north of New Zealand. Because enhanced uptake of CO₂ is linked to a vigorous upper-ocean circulation and to the formation of mode water [DeVries *et al.*, 2017], one interesting question is how much sequestration of CO₂ is in the STMW inventories. As a rough estimate, the maximum peak occurrence of STMW (maximum annual peak occurring in October–November) would hold 4×10^8 kg CO₂ per km² of surface area assuming that 2 grams of CO₂ are dissolved in each 1 kg of water at 16.5° (the mean core layer temperature of the STMW north of New Zealand). The mode water subducts this CO₂ into the thermocline where it will be sequestered. Quantifying carbon sequestration by mode waters [Bates *et al.*, 2002] could be useful for the calculation of the carbon budget because once the mode water subducts the CO₂ is likely to be put in a longer-term storage. Further work is needed to understand the fate of this reservoir.

5. Conclusion

The formation and variability of STMW north of New Zealand was investigated from surface and subsurface temperature observations. The main objectives of this paper were a) to identify the distribution of STMW inventories, b) to investigate potential relationships between the fluctuations observed in the inventories and air-sea heat fluxes and c) to relate the variability of the inventories to that of the EAUC – the subtropical western boundary current along northern New Zealand.

The STMW north of New Zealand has a short lifespan, i.e., there is no longevity and little re-emergence of STMW from 1 year to the next one. This result is different from other STMW regions where anomalous deeper mixed layers may cause STMW inventories to persist for one to two consecutive seasons [Hanawa and Sugimoto, 2004; Sugimoto and Hanawa, 2007].

It was verified that deeper mixed layers lead to increased formation of STMW north of New Zealand. Variability in the mixed layer appears to be driven by fluctuations in air-sea interactions with negative anomalies in heat fluxes associated with deeper mixed layers. However, heat content of the STMW layer is also correlated to the variability of STMW inventories. For example, it was found that increased STMW inventories are linked to negative heat content anomalies; a similar dynamic to that observed in the Gulf Stream region in the North Atlantic Ocean [Kelly *et al.*, 2010] but opposite to the Kuroshio region in the North Pacific [Rainville *et al.*, 2014]. In particular, during the El Niño years, greater STMW inventories coincide with negative ocean heat content anomalies, conversely, lower STMW inventories concur typically with warmer La Niña events when there is lower heat content (positive anomalies) in the STMW layer.

Despite the significant seasonal and interannual variability in STMW inventories, there are no significant trends in water mass properties, including its CLT. This lack of trend is indicative that no major changes in the water mass have occurred in at least the last decade. The variability of the STMW inventories was correlated to the EAUC transports showing some correspondence at interannual time scales. However, if the mechanism connecting the transports and STMW is the movement of the thermocline, the best correspondence occurs when the EAUC transport leads changes in the thermocline depth and STMW inventories by one season, i.e., winter transports are highly correlated with STMW inventories in the following spring. Given the relationship between the current and the water mass it is expected that STMW inventories will tend to

increase (decrease) with increasing (decreasing) transports of the western boundary current north of New Zealand.

To summarize, formation and variability of STMW north of New Zealand appears to be influenced by air-sea interactions with the ocean heat content and dynamics preconditioning for deeper mixed layers and deepening the thermocline.

Acknowledgments

The High Resolution expendable bathythermograph data were made available by the Scripps High Resolution XBT program (<http://www-hrx.ucsd.edu/>). The Argo data were collected and made freely available by the International Argo Program and the national programs that contribute to it. (<http://www.argo.ucsd.edu>, <http://argo.jcommops.org>). The Argo Program is part of the Global Ocean Observing System. The altimeter products were produced by Ssalto/Duacs and distributed by Aviso, with support from Cnes (<http://www.aviso.altimetry.fr/duacs/>). D. F. acknowledges a PhD scholarship from the University of Auckland, New Zealand. This work was supported by the Deep South National Science Challenges, New Zealand. The authors would like to thank the Editor, and to Neil Holbrook and one anonymous reviewer for their helpful comments which improved the manuscript.

References

- Bates, N. R., A. C. Pequignot, R. J. Johnson, and N. Gruber (2002), A short-term sink for atmospheric CO₂ in Subtropical Mode Water of the North Atlantic Ocean, *Nature*, 420(6915), 489–493.
- Ciasto, L. M., and M. H. England (2011), Observed ENSO teleconnections to Southern Ocean SST anomalies diagnosed from a surface mixed layer heat budget, *Geophys. Res. Lett.* 38, L09701, doi:10.1029/2011GL046895.
- de Boyer Montégut, C., G. Madec, A. S. Fischer, A. Lazar, and D. Ludicone (2004), Mixed layer depth over the global ocean: An examination of profile data and a profile-based climatology, *J. Geophys. Res.*, 109, C12003, doi:10.1029/2004JC002378.
- DeVries, T. M., Holzer, and F. Primeau (2017), Recent increase in oceanic carbon uptake driven by weaker upper-ocean overturning, *Nature*, 542(7640), 215–218.
- Dong, S., S. L. Hautala, and K. A. Kelly (2007), Interannual variations in upper-ocean heat content and heat transport convergence in the western North Atlantic, *J. Phys. Oceanogr.*, 37, 11, 2682–2697.
- Douglass, E. M., Y. Kwon, and S. R. Jayne (2013), A comparison of North Pacific and North Atlantic Subtropical Mode Waters in a climatologically-forced model, *Deep Sea Res., Part II*, 91, 139–151.
- Emery, W. J., and R. E. Thomson (2001), *Data Analysis Methods in Physical Oceanography*, Elsevier Sci., 638 pp., Elsevier Sci., Amsterdam.
- Fernandez, D. (2017), Variability, coherence and forcing mechanisms in the New Zealand ocean boundary currents, PhD thesis, 170 pp., Univ. of Auckland, Auckland, N. Z.
- Gordon, N. D. (1986), The southern oscillation and New Zealand weather, *Mon. Weather Rev.*, 114(2), 371–387.
- Goring, D. G., and R. G. Bell (1999), El Niño and decadal effects on sea-level variability in northern New Zealand: A wavelet analysis, *N. Z. J. Mar. Freshwater Res.*, 33(4), 587–598.
- Greig, M. J., N. M. Ridgway, and B. S. Shakespeare (1988), Sea surface temperature variations at coastal sites around New Zealand, *N. Z. J. Mar. Freshwater Res.*, 22(3), 391–400.
- Hanawa, K. (1987), Interannual variations of the winter-time outcrop area of Subtropical Mode Water in the western North Pacific ocean, *Atmos. Ocean*, 25(4), 358–374.
- Hanawa, K., and S. Sugimoto (2004), 'Reemergence' areas of winter sea surface temperature anomalies in the world's oceans, *Geophys. Res. Lett.*, 31, L10303, doi:10.1029/2004GL019904.
- Hanawa, K., and L. Talley (2001), Ocean circulation and climate—Observing and modelling the global ocean; Chapter 5.4 Mode waters, *Int. Geophys.*, 77, 373–386.
- Holbrook, N. J., and A. M. Maharaj (2008), Southwest Pacific Subtropical Mode Water: A climatology, *Prog. Oceanogr.*, 77(4), 298–315.
- Holte, J., and L. Talley (2009), A new algorithm for finding mixed layer depths with applications to Argo data and Subantarctic Mode Water formation*, *J. Atmos. Oceanic Technol.*, 26(9), 1920–1939.
- Hu, H., Q. Liu, X. Lin, and W. Liu (2007), The South Pacific Subtropical Mode Water in the Tasman Sea, *J. Ocean Univ. China*, 6(2), 107–116.
- Huang, R., and B. Qiu (1994), Three-dimensional structure of the wind-driven circulation in the subtropical North Pacific, *J. Phys. Oceanogr.*, 24(7), 1608–1622.
- Iselin, C. O. D. (1939), The influence of vertical and lateral turbulence on the characteristics of the waters at mid-depths, *Eos Trans. AGU*, 20(3), 414–417.
- Kelly, K. A., R. J. Small, R. M. Samelson, B. Qiu, T. M. Joyce, Y. Kwon, and M. F. Cronin (2010), Western Boundary Currents and frontal air–sea interaction: Gulf Stream and Kuroshio Extension, *J. Clim.*, 23, 21, 5644–5667.
- Kobashi, F., and S. Xie (2013), Interannual variability of the North Pacific Subtropical Countercurrent: Role of local ocean–atmosphere interaction, *J. Oceanogr.*, 68, 121–134.
- Kobashi, F., H. Mitsudera, and S. Xie (2006), Three subtropical fronts in the North Pacific: Observational evidence for mode water-induced subsurface frontogenesis, *J. Geophys. Res.*, 111, C09033, doi:10.1029/2006JC003479.
- Kobayashi, S., Y. Ota, and Y. Harada (2015), The JRA-55 reanalysis: General specifications and basic characteristics, *J. Meteorol. Soc. Jpn.*, 93(1), 5–48.
- Kouketsu, S., H. Tomita, E. Oka, S. Hosoda, T. Kobayashi, and K. Sato (2012), The role of meso-scale eddies in mixed layer deepening and mode water formation in the western North Pacific, *J. Oceanogr.*, 68(1), 63–77.
- Li, Z. (2012), Interannual and decadal variability of the subtropical mode water formation in the South Pacific Ocean, *Ocean Modell.*, 47, 96–112.
- McCartney, M. S. (1982), The subtropical recirculation of mode waters, *J. Mar. Res.*, 40, 427–464.
- Mullan, A. B. (1998), Southern hemisphere sea-surface-temperatures and their contemporary and lag association with New Zealand temperature and precipitation, *Int. J. Climatol.*, 18(8), 817–840.
- Qiu, B., and S. Chen (2006), Decadal variability in the formation of the North Pacific Subtropical Mode Water: Oceanic versus atmospheric control, *J. Phys. Oceanogr.*, 36(7), 1365–1380.
- Qiu, B., P. Hacker, S. Chen, K. A. Donohue, D. R. Watts, H. Mitsudera, N. G. Hogg, and S. R. Jayne (2006), Observations of the Subtropical Mode Water evolution from the Kuroshio Extension System Study, *J. Phys. Oceanogr.*, 36(3), 457–473.
- Rainville, L., S. R. Jayne, and M. F. Cronin (2014), Variations of the North Pacific Subtropical Mode Water from direct observations, *J. Clim.*, 27(8), 2842–2860.
- Reynolds, R. W., T. M. Smith, C. Liu, D. B. Chelton, K. S. Casey, and M. G. Schlax (2007), Daily high-resolution-blended analyses for sea surface temperature, *J. Clim.*, 20(22), 5473–5496.
- Roemmich, D., and B. Cornuelle (1992), The subtropical mode waters of the South Pacific Ocean, *J. Phys. Oceanogr.*, 22(10), 1178–1187.
- Roemmich, D., and J. Gilson (2009), The 2004–2008 mean and annual cycle of temperature, salinity, and steric height in the global ocean from the Argo Program, *Prog. Oceanogr.*, 82(2), 81–100.
- Roemmich, D., J. Gilson, J. Willis, P. Sutton, and K. Ridgway (2005), Closing the time-varying mass and heat budgets for large ocean areas: The Tasman Box, *J. Clim.*, 18(13), 2330–2343.

- Sasaki, H., S.-P. Xie, B. Taguchi, M. Nonaka, S. Hosoda, and Y. Masumoto (2012), Interannual variations of the Hawaiian Lee Countercurrent induced by potential vorticity variability in the subsurface, *J. Oceanogr.*, **68**, 93–111.
- Sprintall, J., D. Roemmich, B. Stanton, and R. Bailey (1995), Regional climate variability and ocean heat transport in the southwest Pacific Ocean, *J. Geophys. Res.*, **100**(C8), 15,865–15,871.
- Suga, T., K. Motoki, Y. Aoki, and A. M. Macdonald (2004), The North Pacific climatology of winter mixed layer and mode waters, *J. Phys. Oceanogr.*, **34**(1), 3–22.
- Sugimoto, S., and K. Hanawa (2007), Impact of remote reemergence of the subtropical mode water on winter SST variation in the central North Pacific, *J. Clim.*, **20**(2), 173–186.
- Sugimoto, S., and K. Hanawa (2010), Impact of Aleutian Low activity on the STMW formation in the Kuroshio recirculation gyre region, *Geophys. Res. Lett.*, **37**, L03606, doi:10.1029/2009GL041795.
- Sutton, P. J. H., and D. Roemmich (2001), Ocean temperature climate off north-east New Zealand, *N. Z. J. Mar. Freshwater Res.*, **35**(3), 553–565.
- Talley, L. D., G. L. Pickard, W. J. Emery, and J. H. Swift (2011), *Descriptive Physical Oceanography: An Introduction*, 555 pp., Academic, Amsterdam.
- Taneda, T., T. Suga, and K. Hanawa (2000), Subtropical Mode Water variation in the northwestern part of the North Pacific subtropical gyre, *J. Geophys. Res.*, **105**(C8), 19,591–19,598.
- Tsubouchi, T., T. Suga, and K. Hanawa (2007), Three types of South Pacific Subtropical Mode Waters: Their relation to the large-scale circulation of the South Pacific subtropical gyre and their temporal variability, *J. Phys. Oceanogr.*, **37**(10), 2478–2490.
- Von Storch, H., and F. W. Zwiers (2001), *Statistical Analysis in Climate Research*, 494 pp., Cambridge Univ. Press, Cambridge, U. K.
- Wang, X. H., V. Bhatt, and Y. Sun (2015), Seasonal and inter-annual variability of western Subtropical Mode Water in the South Pacific Ocean, *Ocean Dyn.*, **65**(1), 143–154.
- Yu, K., T. Qu, C. Dong, and Y. Yan (2015), Effect of Subtropical Mode Water on the decadal variability of the subsurface transport through the Luzon Strait in the western Pacific Ocean, *J. Geophys. Res. Oceans*, **120**, 6829–6842, doi:10.1002/2015JC011016.
- Zilberman, N. V., D. H. Roemmich, and S. T. Gille (2014), Meridional volume transport in the South Pacific: Mean and SAM-related variability, *J. Geophys. Res. Oceans*, **119**, 2658–2678, doi:10.1002/2013JC009688.